AEM
Journals.ASM.org

Biofilm Growth and Near-Infrared Radiation-Driven Photosynthesis of the Chlorophyll *d*-Containing Cyanobacterium *Acaryochloris marina*

Lars Behrendt,[a,b] Verena Schrameyer,[c] Klaus Qvortrup,[d] Luisa Lundin,[b] Søren J. Sørensen,[b] Anthony W. D. Larkum,[c] and Michael Kühl[a,c,e]

Marine Biological Section, Department of Biology, University of Copenhagen, Helsingør, Denmark[a]; Section for Microbiology, Department of Biology, University of Copenhagen, Copenhagen, Denmark[b]; Plant Functional Biology and Climate Change Cluster, School of the Environment, University of Technology Sydney, Sydney, Australia[c]; Department of Biomedical Sciences, University of Copenhagen, Copenhagen, Denmark[d]; and Singapore Centre on Environmental Life Sciences Engineering, School of Biological Sciences, Nanyang Technological University, Singapore[e]

The cyanobacterium *Acaryochloris marina* is the only known phototroph harboring chlorophyll (Chl) *d*. It is easy to cultivate it in a planktonic growth mode, and *A. marina* cultures have been subject to detailed biochemical and biophysical characterization. In natural situations, *A. marina* is mainly found associated with surfaces, but this growth mode has not been studied yet. Here, we show that the *A. marina* type strain MBIC11017 inoculated into alginate beads forms dense biofilm-like cell clusters, as in natural *A. marina* biofilms, characterized by strong O_2 concentration gradients that change with irradiance. Biofilm growth under both visible radiation (VIS, 400 to 700 nm) and near-infrared radiation (NIR, ~700 to 730 nm) yielded maximal cell-specific growth rates of 0.38 per day and 0.64 per day, respectively. The population doubling times were 1.09 and 1.82 days for NIR and visible light, respectively. The photosynthesis versus irradiance curves showed saturation at a photon irradiance of E_k (saturating irradiance) >250 μmol photons m^{-2} s^{-1} for blue light but no clear saturation at 365 μmol photons m^{-2} s^{-1} for NIR. The maximal gross photosynthesis rates in the aggregates were ~1,272 μmol O_2 mg Chl d^{-1} h^{-1} (NIR) and ~1,128 μmol O_2 mg Chl d^{-1} h^{-1} (VIS). The photosynthetic efficiency (α) values were higher in NIR-irradiated cells [(268 ± 0.29) × 10^{-6} m^2 mg Chl d^{-1} (mean ± standard deviation)] than under blue light [(231 ± 0.22) × 10^{-6} m^2 mg Chl d^{-1}]. *A. marina* is well adapted to a biofilm growth mode under both visible and NIR irradiance and under O_2 conditions ranging from anoxia to hyperoxia, explaining its presence in natural niches with similar environmental conditions.

The cyanobacterium *Acaryochloris marina* is unique among phototrophs because it has largely replaced chlorophyll *a* (Chl *a*) in its photosystems with Chl *d*. It is reasonably easy to cultivate *A. marina* as suspended (planktonic) cultures in minimal or enriched medium (31, 32). Due to its unique possession of Chl *d*, such *A. marina* cultures have been the subject of a number of detailed studies, including studies of its genome (32, 47), its basic photophysiology (2, 8, 49, 50), Chl *d* biosynthesis (45), chromatic photoacclimation (18), pigment composition (1, 9), and ultrastructure (28, 48). A recent study also demonstrated the presence and activity of N_2 fixation under hypoxic conditions in a culture of the *A. marina* strain HICR111A (36).

In contrast, *A. marina*'s ecology and natural habitats are much less studied, but it is mostly reported from surface-associated habitats and has been shown to form aggregates of cells in biofilms. Examples of such *A. marina*-containing biofilms are the underside of the tropical ascidian *Lissoclinum patella* (22) and endolithic microbial communities (6) depleted of visible radiation (VIS, 400 to 700 nm) and enriched in near-infrared radiation (NIR, >700 nm). While naturally occurring cells of *A. marina* apparently prefer to grow associated with surfaces, laboratory investigations of the growth and NIR-dependent photosynthesis of *A. marina* strains in biofilms are lacking.

While planktonic growth occurs under more homogeneous and less dynamic conditions, microbes in photosynthetic biofilms experience steep gradients in O_2, pH, nutrient availability, light, and temperature due to a high volume-specific metabolic activity coupled with mass transfer limitation by diffusive transport in the dense matrix of cells and exopolymers (23). Changes in irradiance or substrate supply lead to fast dynamic shifts in the physicochemical conditions in biofilms over short time intervals (seconds to minutes). Protection against environmental stress, greater nutrient availability, and acquisition of new genetic traits through horizontal gene transfer are some of the suggested advantages of growing in a biofilm (13), yet many of these proposed benefits remain untested.

Marked differences between planktonic and biofilm growth modes have been observed in bacterial pathogens (15, 16, 38, 44, 53), green algae (19, 43), and yeast (54). In these organisms, the difference in growth forms is reflected in their physiology, gene expression, phenotypic plasticity, and functional characteristics. Therefore, extrapolation of data retrieved from planktonic cultures to natural systems can be difficult (12, 13), highlighting the need to conduct ecologically relevant experiments in the appropriate growth mode.

Biofilm-like growth conditions can be mimicked by incorporating cells into a matrix, such as alginate (52). This forces the entrapped cells to grow in close proximity to each other in a mass transfer-limited matrix, effectively creating microenvironmental conditions similar to those in naturally occurring biofilms. Accordingly, the employment of such immobilization may be of assistance to establish reproducible experimental systems that pro-

Received 9 February 2012 **Accepted** 20 March 2012
Published ahead of print 30 March 2012
Address correspondence to Michael Kühl, mkuhl@bio.ku.dk.

doi:10.1128/AEM.00397-12

vide metabolic measures under closer approximation to the biofilm growth mode. In this study, we employed such alginate immobilization to study the biofilm-like growth and photosynthetic activity of the Chl *d*-containing cyanobacterium *A. marina*. Cell growth was monitored using flow cytometric cell counts, chlorophyll content, and imaging by microscopy. Simultaneous measurements of gross photosynthesis and effective quantum yields were performed to gain information on the photosynthetic competence and efficiency of immobilized *A. marina*.

MATERIALS AND METHODS

***Acaryochloris marina* growth conditions.** *Acaryochloris marina* strain MBIC11017 was grown in 200-ml cell culture flasks with KESM medium (salinity of 30) on a shaking incubator at 28°C as previously reported (30). The cultures were shaken at 100 rpm under a 12-/12-h light-dark period. Near-infrared radiation (NIR) was provided by narrow-band light-emitting diodes (LEDs) (centered at 720 nm) (Epitex, Inc., Japan) at an irradiance of 20 to 40 μmol photons m^{-2} s^{-1}. Another set of cultures were grown under the same irradiance but using visible light delivered by a halogen lamp (HQ Power; Brinck Electronic, Denmark). Planktonic and immobilized *A. marina* cells were grown under the same light and temperature conditions.

Alginate bead preparation and sampling. Beads were prepared using alginate extracted from the brown alga *Laminaria hyperborea* (Protanal LF 10/60; FMC Biopolymer, Drammen, Norway) using a wt/vol ratio of 4.9%. For 100 ml of alginate solution, 4.9 g of Protanal LF 10/60 was suspended in 70 ml of MilliQ water and stirred on a hotplate set to 50°C until dissolved, after which the remaining 30 ml of water was added. The alginate solution was subsequently autoclaved at 120°C for 20 min.

For bead preparation, 15 ml of the alginate solution was mixed with 5 ml of pregrown planktonic *Acaryochloris marina* culture exhibiting an optical density of 0.5 at 750 nm. Additionally, cells were counted using a Thoma-hemocytometer (Blaubrand GmbH, Germany) and diluted to a concentration of 1.0×10^7 cells ml^{-1} alginate solution. The alginate-culture solution was vortexed for ~45 s at the highest speed and then transferred into a sterile 20-ml syringe. The syringe was placed into a syringe pump (Aladdin 220; World Precision Instruments, Sarasota, FL) and connected to a 0.5-mm-wide and 60-mm-long sterile hypodermic needle using sterile tubing. The injection needle was placed 3 cm above a sterilized 250 ml beaker filled with 150 ml of prewarmed (28°C) 4% $SrCl_2$ solution, previously reported to yield beads of the necessary stability for long-term incubation in high-salinity seawater (33). The solution was stirred at 150 rpm, and the syringe pump was set at a delivery rate of 1 ml min^{-1}, corresponding to a formation of ~1 bead s^{-1}, with the spherical beads having a final diameter of 2.52 ± 0.17 mm (mean ± standard deviation). The beads were hardened in the $SrCl_2$ solution for 45 min and were then washed three times with deionized water (Maxima; Holm & Halby, Denmark) to remove any remaining $SrCl_2$. After washing, the beads were placed into prewarmed KESM medium (28°C) and grown under the same conditions as planktonic cultures with the exception that the medium was changed every 4th day.

Beads were sampled in technical triplicates every 96 h by use of a sterile plastic syringe, placed into microcentrifuge tubes, and immediately transferred into a −80°C freezer for later chlorophyll extraction and flow cytometric analysis.

Chlorophyll extraction and spectrophotometry. Aliquots of 20 frozen beads were dissolved in 0.5 M Tri-Na-citrate (pH 6.5) for 20 min and homogenized with a sterile micropestle. Cells were centrifuged at 5,000 × *g* for 10 min, the supernatant removed, and the resulting pellet resuspended in 96% ethanol and incubated at 4°C for 30 min. During incubation, the samples were resuspended with a sterile micropestle every 15 min. The alginate was pelleted by centrifugation at 5,000 × *g*, and the supernatant was used to determine Chl *d* and Chl *a* concentrations spectrophotometrically according to the method in reference 41, using a scanning spectrophotometer (UV-2101PC; Shimadzu, Japan). The chlorophyll content of the beads was calculated in mg cm^{-3}, assuming a perfect sphere and even distribution of chlorophyll across individual beads. To prevent bleaching of the photopigments, all handling was done as quickly as possible and under low irradiance.

Flow cytometry. Aliquots of 20 frozen beads were dissolved in a manner similar to that described for chlorophyll extraction, with the addition of a 30-min sonication step (Bransonic 1510 sonicator; Danbury, CT) after treatment with 0.5 M Tri-Na-citrate (pH 6.5). Following sonication, the cells were filtered through a nylon syringe filter with a mesh size of 10 μm (Frisenette ApS, Denmark) in order to remove any residual alginate. All flow cytometric analyses were performed on a FACSAria III (BD Biosciences, United States), using a 488-nm laser in conjunction with the BD FACSFlow sheath fluid (BD Biosciences, United States). Voltages were set at 140 V for forward scatter (FSC) and 360 V for side scatter (SSC). All parameters were expressed on a logarithmic scale. Flow rates (μl min^{-1}) were determined as previously described (27), and the average flow rate was calculated based on three replicates: before, during, and after enumeration of cells in the samples. Samples were mixed by vortexing, and all gated events were counted for 1 min at flow rate 1, where gates were established based upon FSC and SSC population characteristics. The collected data were analyzed using the software package BD FACSDiva (BD Biosciences, United States). Cell-specific growth rates (μ) and corresponding population doubling times were calculated using the linear increase in cell abundance as determined by semi-log plotting.

Light calibration. Absolute irradiance measurements of NIR from the LED light sources were performed using a calibrated spectrometer (Jaz; Ocean Optics, Dunedin, FL), where photon irradiance was integrated over a spectral range from 650 to 800 nm. Different NIR irradiances were administered by altering the distance of three collimated NIR LEDs (700 to 740 nm centered at 730 nm) (Roithner Lasertechnik, Vienna, Austria) to the sample. A pulse-amplitude-modulated (PAM) fluorometer (JuniorPAM, Walz GmbH, Germany) was used to administer defined levels of blue actinic light via an optical fiber (1.5 mm diameter); irradiance levels were calibrated with a mini-quantum scalar irradiance sensor (Walz GmbH, Effeltrich, Germany) connected to a quantum irradiance meter (LiCor-250; LiCor, Inc., Lincoln, NE). Ambient light was excluded by covering the experimental setup with black cloth.

Microsensor measurements. Single beads were immobilized on a piece of black neoprene with thin stainless steel insect preparation needles and submerged in a flow chamber flushed with preheated artificial seawater (28°C, salinity of 30, Marine Environment; Aquacraft, San Carlos, CA). The water was circulated through the flow chamber from an aerated reservoir by means of a submerged water pump.

A Clark-type O_2 microsensor (tip size, ~20 μm [39]) was mounted on a motorized micromanipulator (Pyro-Science GmbH, Aachen, Germany) and connected to a picoammeter (Unisense PA2000; Unisense A/S, Aarhus, Denmark). The sensor was linearly calibrated from measurements in O_2-free seawater (by the addition of sodium dithionite) and fully aerated seawater at the experimental temperature and salinity. As the alginate beads were flexible and easily compressed, the beads were first carefully punctured by inserting the microsensor to a depth of approximately 1.5 mm; upon retraction, the elastic alginate matrix sealed the hole. For all subsequent microprofiling, the sensor was then inserted into the same position. The position where the microsensor tip touched the bead surface was determined by visual inspection using a stereomicroscope mounted on a stand in front of the aquarium. All microsensor signals were recorded on a strip chart recorder (Kipp and Zonen, B.V., Delft, Netherlands) and via an analog-to-digital (A/D) converter (AD-216; Unisense A/S, Aarhus, Denmark) connected to a personal computer (PC) running data acquisition and micromanipulator-positioning software (Profix; Pyro-Science GmbH, Aachen, Germany).

Variable chlorophyll fluorescence measurements. A pulse amplitude-modulated (PAM) fluorometer (Junior-PAM; Walz GmbH, Effeltrich, Germany), placed with the 1.5-mm-wide measuring fiber situated close to the bead surface, was used to investigate the photosynthetic activ-

ity of *A. marina* beads via variable chlorophyll fluorescence analysis. A detailed description of such analysis and the measuring principles is beyond the scope of this report and has been described elsewhere (5, 37, 46). Using the saturation pulse method (5, 46), the maximum quantum yield of photosystem II [$(\Phi PSII)_{max}$] photosynthetic energy conversion, $(\Phi_{PSII})_{max} = (F_m - F_0)/F_m$, was measured after dark incubation and the light-adapted effective quantum yield of PSII, $\Phi_{PSII} = (F'_m - F)/F'_m$, was measured at defined levels of actinic irradiance. In these equations, F_0 and F denote the minimal fluorescence yields of PSII in darkness and under actinic light illumination, respectively, while F_m and F'_m denote the maximal fluorescence yields of PSII as measured under a strong saturating light pulse in darkness and under actinic light illumination, respectively. The PSII-driven relative electron transport rates (rETR) were calculated with the formula rETR = $\Phi_{PSII} \times$ PAR (photosynthetically active radiation). To investigate light acclimatization, rETR-versus-quantum irradiance curves were determined in beads previously incubated under defined levels of either NIR or blue light. Actinic blue light was provided through the Junior-PAM fiber, whereas calibrated levels of NIR were provided by LEDs.

Combined chlorophyll fluorescence and O_2 evolution measurements. For simultaneous measurements of O_2 concentration and variable chlorophyll fluorescence, the beads were mounted in the flow chamber as described above. The Junior-PAM measuring fiber was situated close to the bead surface and was used to measure variable chlorophyll fluorescence and to provide blue actinic light. Gross photosynthesis (in units of nmol O_2 cm^{-3} s^{-1}) was measured using the O_2 microsensor light-dark shift method (23, 40) with the tip at a suitable distance within the bead. Gross photosynthesis measurements were subsequently normalized to volume-specific Chl *d* contents found in single beads and calculated into units of μmol O_2 mg Chl d^{-1} h^{-1}. Consecutive to the light-dark shift, variable chlorophyll fluorescence was determined by applying three saturation pulses for 0.8 s at 10-s intervals with an irradiance of ~8,000 μmol photons m^{-2} s^{-1}. Besides measurements with blue actinic light, similar measurements were also done with defined levels of NIR light delivered from LEDs. More details on variable chlorophyll fluorescence measurements in combination with O_2 microsensor measurements of gross photosynthesis can be found in reference 51.

Light microscopy. Beads were cut in half using a razorblade and mounted on microscopy slides with the cut surface facing down. Imaging was performed with a coolSNAP camera (Photometrics, Tucson, AZ) mounted on a Zeiss Axioscope 2 plus microscope (Zeiss GmbH, Jena, Germany), using either ×10 or ×40 magnification. Images were recorded at the same time as sampling for flow cytometric analysis, and chlorophyll extraction was performed (approximately every 96 h).

SEM. Comparative scanning electron microscopy (SEM) analysis was performed on bead cross sections and *A. marina*-containing biofilm samples from the underside of the didemnid ascidian *Lissoclinum patella* (see details of sampling in reference 7). Following a rinse in distilled water, cross sections of beads and biofilms isolated from *Lissoclinum patella* were first dehydrated with 100% ethanol according to standard procedures and were then subjected to critical-point drying (Balzers CPD 030; Balzers, Switzerland) using CO_2. The beads were subsequently mounted on stubs using colloidal coal as an adhesive and sputter coated with gold (SEM coating unit E5000; Polaron). Beads were examined with an XL FEG 30 (Philips, Netherlands) scanning electron microscope operated at an accelerating voltage of 2 kV.

RESULTS

Artificial and natural biofilms of *A. marina* show similar characteristics. Beads inoculated with *A. marina* became visibly green due to growth and accumulation of chlorophyll over a 5-week incubation period (Fig. 1A). Light microscopy of cross-sectioned beads demonstrated a typical growth pattern for immobilized cells: growth started with a few dividing cyanobacteria, the matrix expanded in order to accommodate the additional cells, dense clusters of cyanobacteria were formed, and the expansion of the clusters finally reached the outer perimeter of the alginate matrix, where *A. marina* cells started to leak into the surrounding medium (Fig. 1B, days 0 to 32). Growth of other, unidentified bacteria was observed in immobilized cells grown under visible light but not in those grown under NIR. Visual inspection of *A. marina* cell clusters within the alginate matrix showed no further increase in their size after 32 days in both light treatments. Growing the cells for an additional 14 days (data not shown) revealed no additional increase in cell cluster size.

The SEM investigation of immobilized cells in the alginate beads showed cells of approximately 1 to 2 μm in size growing in dense clusters within the alginate matrix (Fig. 2A, C, and E). Growth of other bacteria was not noticed in beads kept under NIR (Fig. 2A and C) but was frequently observed in beads grown under visible light (Fig. 2E). SEM imaging of the underside of the didemnid ascidian *Lissoclinum patella*, a natural habitat of *A. marina* (7), showed cells of approximately the same size as the cultured *A. marina* cells (1 to 2 μm) (Fig. 2B, D, and F). Clusters of *A. marina*-like cells were frequently found in places where the ascidian test material folded or where other three-dimensional structures occurred.

Wavelength-dependent photopigment production and cell growth. Alginate-embedded *A. marina* cells grown under NIR exhibited approximately 2-fold higher Chl *d* concentrations than cells grown under visible light (Fig. 3A). Maximal Chl *d* concentration was observed after 39 days in beads grown under visible light (2.28 ± 0.8 μg Chl *d* $bead^{-1}$; $n = 3$) and 48 days with NIR (5.88 ± 0.4 μg Chl *d* $bead^{-1}$; $n = 3$). The concentration of Chl *a* was not affected by the growth incubation wavelength (visible light, 0.19 ± 0.08 μg Chl *a* $bead^{-1}$, $n = 3$, and NIR, 0.19 ± 0.01 μg Chl *a* $bead^{-1}$, $n = 3$, at day 40) (Fig. 3B).

Flow cytometric cell counts of *A. marina* revealed that immobilized cells reached higher maximum cell densities when grown under NIR [(2.83 ± 0.005) × 10^8 cells $bead^{-1}$ at 48 days, $n = 3$] (Fig. 3C) than under visible light [(1.46 ± 0.11) × 10^8 cells $bead^{-1}$ at 47 days, $n = 3$]. The per-cell content of chlorophyll under visible light was 0.07 pg $cell^{-1}$ (Chl *d*) and 0.017 pg $cell^{-1}$ (Chl *a*). Higher Chl *d* concentrations were obtained for immobilized cells grown under NIR (0.2 pg $cell^{-1}$), while the Chl *a* per-cell content was found to be lower (0.007 pg $cell^{-1}$) (Table 1). Accordingly, Chl *a*/*d* ratios were >10-fold higher in immobilized cells grown under visible light (0.229) than under NIR (0.033). Based on the linear increase of cell numbers displayed in Fig. 3C, we calculated maximum cell-specific growth rates of 0.64 and 0.38 for NIR and visible light, respectively (Table 1). The corresponding population doubling times were 1.09 days (NIR) and 1.82 days (VIS).

Wavelength-dependent O_2 evolution and photosystem saturation. Oxygen profiling in NIR-irradiated beads demonstrated maximum O_2 production at a depth of ~400 to 600 μm (Fig. 4). Gross photosynthesis (*P*) measurements, using either blue or NIR light, were performed by positioning the O_2 microelectrode tip at this depth and performing experimental light-dark shifts with the sensor remaining in place. *P* was normalized to the Chl *d* concentration within one bead (mg cm^{-3}), yielding final units of μmol O_2 mg^{-1} Chl *d* h^{-1}. Maximum gross photosynthesis (P_{max}) rates were on the order of ~1,272 μmol O_2 mg Chl d^{-1} h^{-1} ($n = 1$) and ~1,128 ± 568 ($n = 3$) μmol O_2 mg Chl d^{-1} h^{-1} for NIR and blue light, respectively (Table 1). No saturation of *P* was observed when beads were illuminated with the maximum NIR irradiance possi-

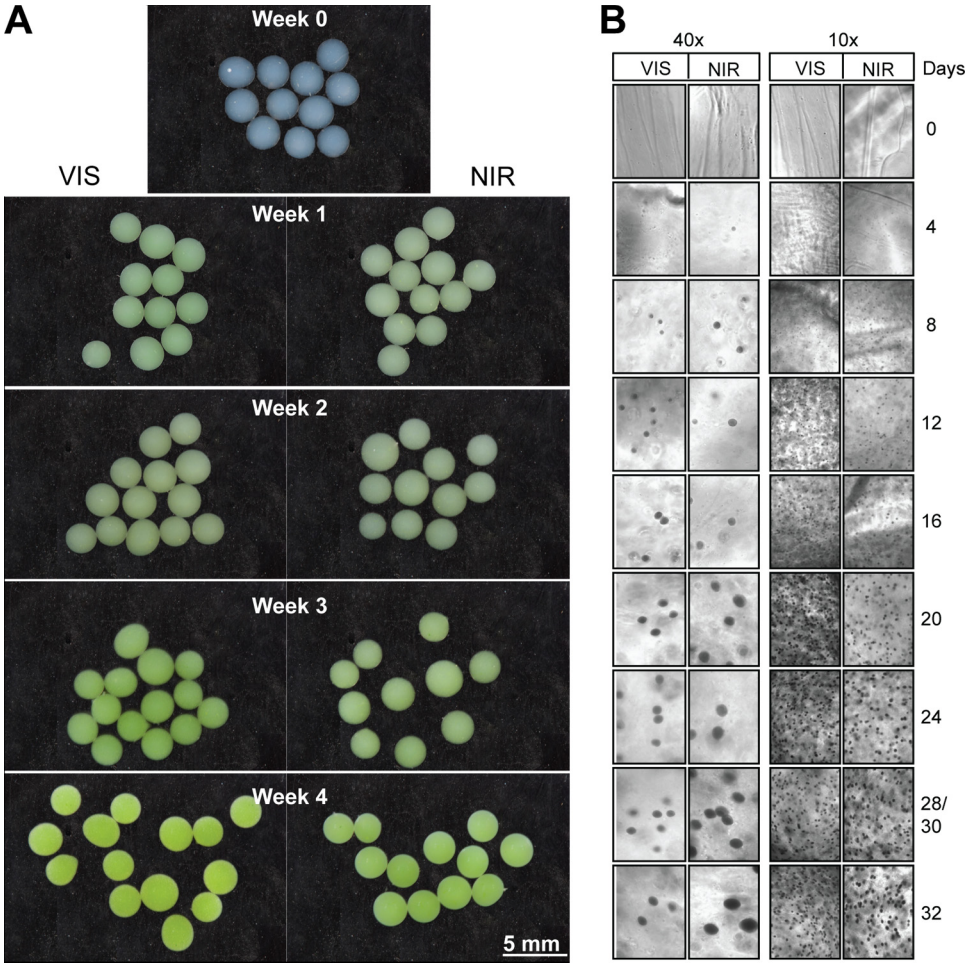

FIG 1 Visual representation of *Acaryochloris marina* growth in alginate beads. Beads were grown under either near-infrared radiation (NIR) or visible light (VIS). (A) Macroscopic imaging of *A. marina* growing in alginate over 5 weeks. (B) Light micrographs of bead cross sections. Images of cross sections were recorded using ×10 or ×40 magnification. Beads were sampled every 4th day with the exception of days 28 and 30, when only NIR (day 28) or VIS beads (day 30) were sampled.

ble (365 μmol photons m^{-2} s^{-1}) (Fig. 5A, NIR), whereas blue light saturated *P* at an irradiance of 144 μmol photons m^{-2} s^{-1} (Fig. 5A, blue light).

The onset of saturation, as determined through variable chlorophyll fluorescence measurement of rETR, was observed at a photon irradiance of ~250 μmol photons m^{-2} s^{-1} of blue light (Fig. 5B, blue light), while no onset of saturation was observed for beads previously irradiated with NIR (Fig. 5B). Despite a lower photon irradiance, an ~40% higher rETR was recorded when immobilized cells were irradiated with the maximum NIR irradiance (rETR, ~162 ± 10, $n = 3$) than in those given blue light at a maximal irradiance (rETR, ~115 ± 14, $n = 3$). Gross photosynthesis-versus-irradiance data (Fig. 5A) were used to calculate the relative photosynthetic efficiency (α) from the initial slope of the *P* versus *E* curves (Table 2). The α values were found to be higher in beads irradiated with NIR [$(268 \pm 0.29) \times 10^{-6}$ m^2 mg Chl d^{-1}, $n = 3$] than in those irradiated with blue light [$(231 \pm 0.22) \times 10^{-6}$ m^2 mg Chl d^{-1}, $n = 3$].

DISCUSSION

The underside of didemnid ascidians is one of the few habitats of *A. marina* that has been described in terms of its light and O_2 microenvironment; here *Acaryochloris* grows in dense clusters interspersed with a diverse community of other microbes in a microniche enriched in NIR and depleted of visible light while experiencing irradiance-dependent shifts between anoxic and hyperoxic conditions (7, 22, 24). The same preference of *A. marina* for NIR-enriched environments was shown in an endolithic microenvironment (6), and a global distribution of Chl *d*-containing cyanobacteria in such niches was hypothesized (6, 20). Due to its unique photosynthetic apparatus, with Chl *d* dominating both PSII and PSI, the interest in *A. marina* has grown substantially, and laboratory-based studies have revealed many new insights into the limits of oxygenic photosynthesis. To our knowledge, all of these studies have been performed using planktonic cultures and have, as such, dismissed the naturally occurring growth state of *A. marina*. Our study is the first attempt at studying cells of *A. marina* under conditions mimicking their natural surface-associated growth mode, by embedding cells into an alginate matrix. We followed the growth of immobilized *A. marina* cells using imaging, photopigment extraction, and microsensor measurements.

Microscopy. The growth of immobilized *A. marina* cells closely resembled the previously reported growth of alginate-im-

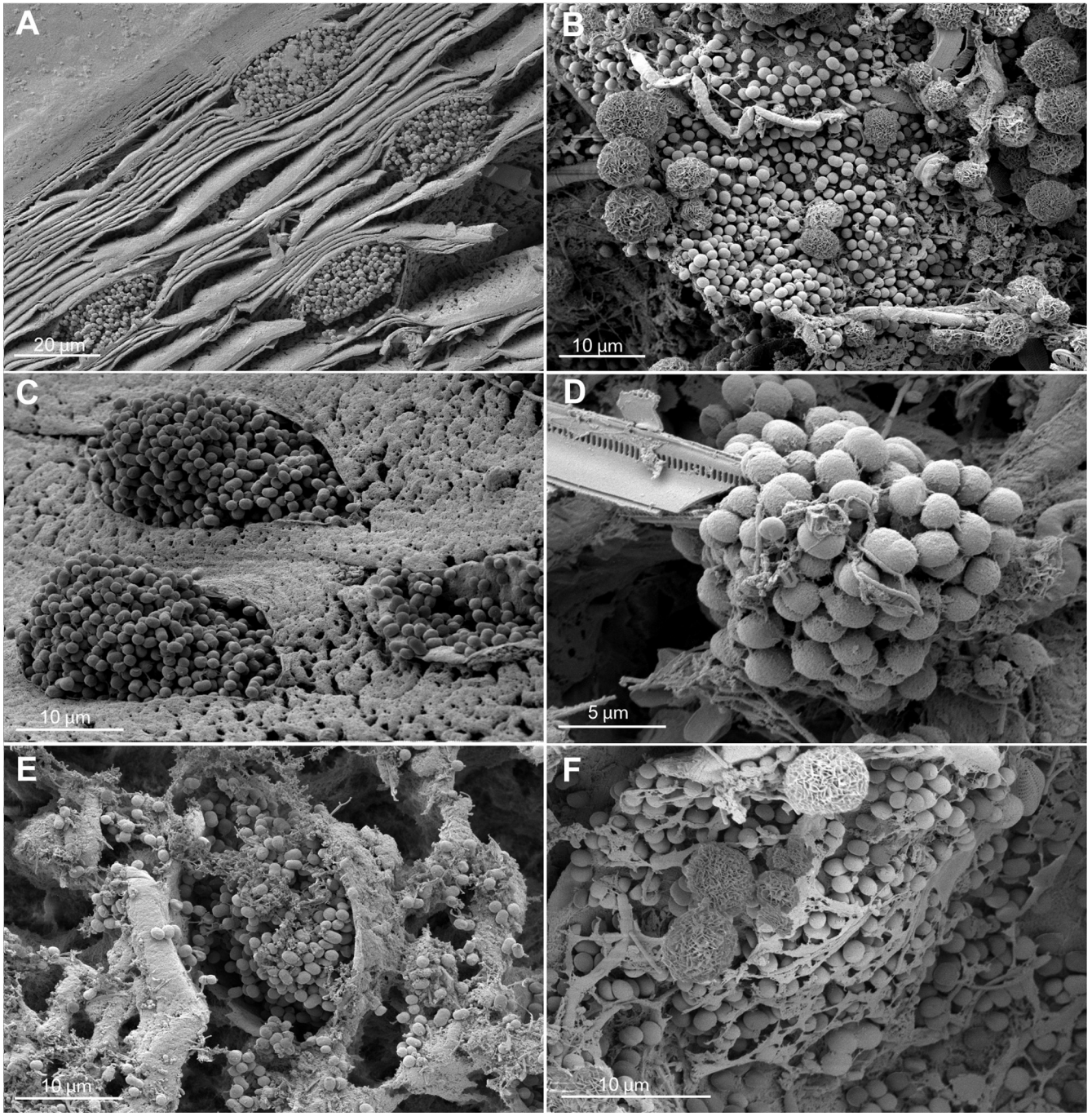

FIG 2 Scanning electron micrographs of cross sections through alginate beads with immobilized *A. marina* cells (A, C, and E) and naturally occurring biofilms from the underside of the didemnid ascidian *Lissoclinum patella* (B, D, and F). (A, C) Typical cell clusters of *A. marina* growing within the alginate matrix; note the laminar layers of alginate enclosing the cell clusters. (E) Growth of unidentified bacteria in alginate beads kept under visible light. (B, D, F) naturally occurring biofilms found on the underside of the didemnid ascidian *L. patella*; note the round *A. marina*-like cells (1 to 2 μm in size) that closely resemble *A. marina* cells growing in alginate (see A, C, and E).

mobilized bacteria and microalgae (55): immediately after inoculation, a few individual cells are dispersed throughout the matrix, and over time these cells grow into larger microcolonies that increase in size and cause expansion of the surrounding alginate. Eventually these microcolonies reach the outer surface of the bead, where they rupture it and release cells into the surrounding medium. This leakage is supported by alginate bead growth models (56) and by observations from immobilized microalgae (25). SEM of biofilms sampled from the underside of the didemnid ascidian *Lissoclinum patella* (7) revealed dense clusters of cells, approximately 1 to 2 μm in size, closely resembling previously reported sizes and micrographs of *A. marina*-like cells (6, 14, 32).

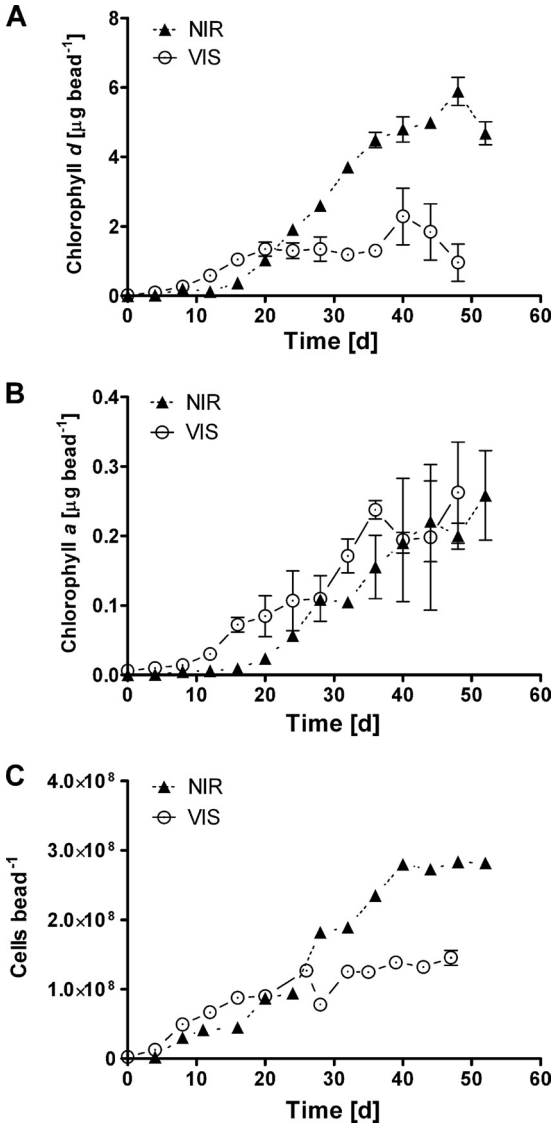

FIG 3 Pigment and cell concentrations of alginate-embedded *A. marina*. VIS, cells grown under visible light; NIR, cells grown under near-infrared LEDs. All data shown are based on technical triplicates; error bars denote the standard deviation from the mean. (A) Chlorophyll *d* concentration of cells grown under visible light and NIR. (B) Chlorophyll *a* concentration of cells grown under NIR and visible light. (C) Cell counts per single bead as determined by flow cytometry where cells were sorted based on size and fluorescence.

Comparison with SEM images of the artificially immobilized *A. marina* cells revealed a high similarity, indicating that alginate embedment provides a good natural growth model for *A. marina*. Growth of other, unidentified bacteria was observed in beads imaged with SEM. This was expected, as most *A. marina* cultures are known to be nonaxenic (32, 48). Surprisingly, growth of these unidentified bacteria was only observed in beads kept under visible light and not in those kept under NIR. We did not further characterize these bacteria, which were relatively low in numbers, but their apparently wavelength-dependent growth suggests that they may be phototrophs unable to use NIR. Additionally, embedded *A. marina* cells grew to higher densities under NIR. Both of these aspects would enable *A. marina* to outcompete other members in the nonaxenic culture, and we speculate that repeated immobilization combined with incubation under NIR could thus be used for obtaining pure cultures of *A. marina*.

Photopigment analysis. The blue and NIR light used in our experiments can be absorbed by chlorophylls (i.e., ~440/675 nm for Chl *a* and ~480/715 nm Chl *d*), enabling *A. marina* to use blue light, NIR, and other wavelengths of PAR for light harvesting and growth under different light sources. Two studies of *A. marina* reported doubling times in planktonic cultures under visible light ranging from 55 to 70 h (48) to 33 to 87 h (18), corresponding to 2.2 to 2.9 days and 1.3 to 3.6 days. These growth rates are comparable to the doubling times in biofilms obtained in this study (1.09 and 1.82 days for NIR and visible light, respectively). In terms of photopigment content, we found that alginate-embedded cells grown under NIR produced approximately twice as much Chl *d* as those exclusively grown under visible light. The Chl *a* concentrations measured in immobilized cells grown under visible light and NIR were remarkably similar (0.19 µg Chl *a* bead^{-1} at day 40 for both), highlighting the importance of Chl *d* for both light harvesting and photosynthesis in *A. marina*. In *A. marina*, Chl *a* has essentially been displaced by Chl *d* as the main photosynthetic pigment (10, 11, 24, 34, 48–50) and its functional role appears more related to Chl *d* biosynthesis (45) and charge recombination in photosystem II (50). Photoacclimation in the *A. marina* type strain MBIC11017 appears to be performed through alterations of Chl *a*/*d* ratios under high-light (10, 32) and low-light (18, 48) conditions, while chromatic photoacclimation in *A. marina* was reported to involve regulation of its phycobiliprotein content (17). The Chl *a*/*d* ratios for immobilized cells grown under NIR were surprisingly similar (in our study, 0.0339) to previously published results (0.0346), where *A. marina* was grown under red light (18). Immobilized cells exposed to visible light (20 to 40 µmol photons m^{-2} s^{-1}) had substantially higher Chl *a*/*d* ratios (0.229) than reported by Gloag et al. (0.0393 at ~5 µmol photons m^{-2} s^{-1} and 0.0552 at ~100 µmol photons m^{-2} s^{-1}) (18) and were approximately twice as high as those reported in reference 32. Higher chlorophyll concentrations are commonly found in immobilized microalgae than in planktonic growth (25, 35). Our observed change in Chl *a*/*d* ratios could, however, also be related to self-shading effects of cell clusters throughout the beads (25), and higher chlorophyll concentrations do not necessarily relate to higher biomass but may rather represent acclimation to such self-shading within the beads.

TABLE 1 Growth and photosynthesis parameters for alginate-embedded *Acaryochloris marina* cells[a]

Parameter	NIR	VIS	Blue light
Maximum growth rate (µ)	0.64	0.38	
Population doubling time (*d*)	1.09	1.82	
Cells per bead	1.46×10^8 (day 47)	2.85×10^8 (day 48)	
Chl *a* per cell (pg)	0.0070	0.0175	
Chl *d* per cell (pg)	0.2077	0.0767	
Chl *a*/*d* ratio	0.0339	0.2290	
P_{max} (µmol O_2 mg Chl d^{-1} h^{-1})	1,272		1,128 ± 568

[a] All measurements are based on the average values of three technical replicates.

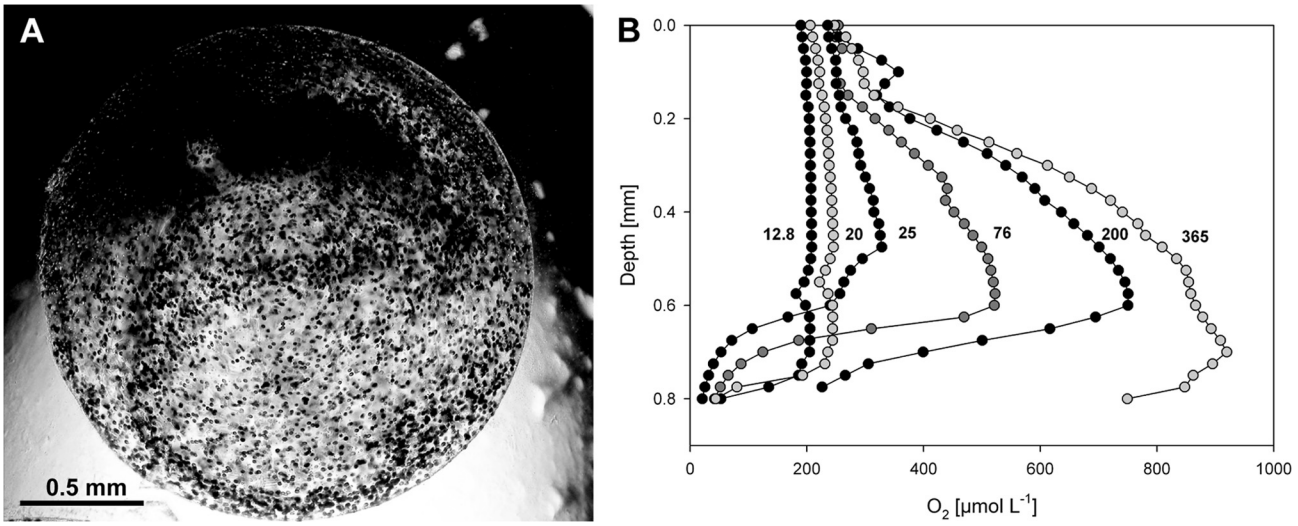

FIG 4 (A) Cross section of an approximately 4-week-old alginate bead with clearly visible clusters of *A. marina* cells. (B) Oxygen concentration microprofiles measured with a Clark-type O_2 microsensor. Oxygen concentrations (in μmol liter^{-1}) were measured at increasing depths under six different NIR irradiance levels (13, 20, 25, 76, 200, and 365 μmol photons m^{-2} s^{-1}). Microprofiles represent average values from three technical replicates.

By assuming an equal distribution of photopigment throughout the bead, we found that the per-cell Chl *d* concentration reached values of 0.2 pg Chl *d* cell^{-1} under NIR and 0.07 pg Chl *d* cell^{-1} when grown under visible light. A study on planktonic cells of *A. marina* (18) demonstrated comparable pigment levels for cells grown under visible light (0.03 to 0.05 pg Chl *d* cell^{-1}) but much lower values in cells exposed to red light (0.058 pg Chl *d* cell^{-1}). Gloag et al. (18) used tinted window glass for their growth experiments (30% transmission, >650 nm), and as Chl *d* absorbs maximally at 710 to 715 nm, higher Chl *d* yields were expected in immobilized cells grown under monochromatic NIR centered at 720 nm.

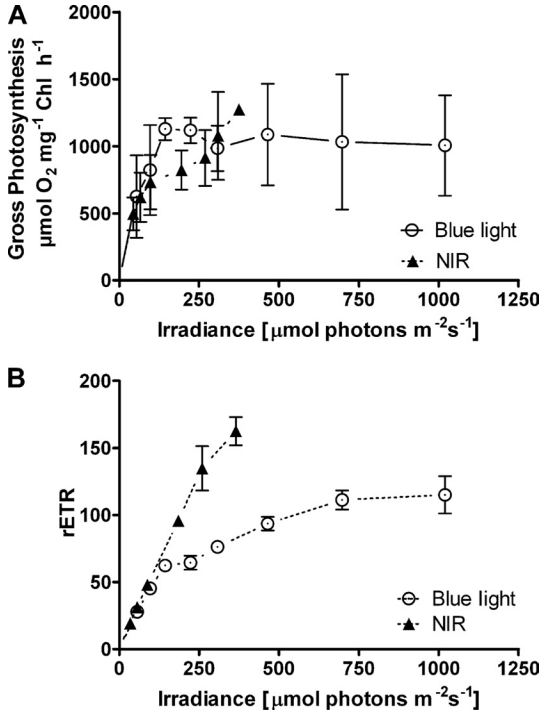

FIG 5 Photosynthesis of *A. marina* in alginate beads. (A) Gross photosynthesis was measured with an O_2 microsensor placed at a depth of 2 to 500 μm using the light-dark shift method. NIR was administered in increasing intensities by altering the distance of three collimated LEDs to the beads, while blue light was provided through an optical fiber placed directly at the bead surface. (B) Relative electron transport rates (rETR) measured on the bead surface using a fiber-optic PAM fluorometer. rETR was measured after a steady-state condition for O_2 production under either NIR or blue light was observed. Three independent biological replicates were used to generate the data displayed in panels A and B.

Photosynthetic activity and efficiency. The initial linear slope of *P* versus irradiance curves, α, was used to assess the relative photosynthetic efficiency of immobilized *A. marina* cells. We found α values for immobilized *A. marina* cells irradiated with blue light that were lower than the α values determined under NIR illumination. Similar effects were shown for red light illumination in a study of planktonic *A. marina* (18). The α values for planktonic cells (298×10^{-6} m^2 mg Chl d^{-1}, grown under visible light) (18) were similar to the numbers obtained from another study using a waiting-in-line model (205×10^{-6} m^2 mg Chl d^{-1}) (42) and were overall comparable to the α values obtained for immobilized cells irradiated with blue light in our study [$(231 \pm 0.22) \times 10^{-6}$ m^2 mg Chl d^{-1}]. The values of P_{max} for immobilized *A. marina* cells were calculated to be ~1,128 μmol O_2 mg Chl d^{-1} h^{-1} for blue light and ~1,272 μmol O_2 mg Chl d^{-1} h^{-1} for NIR. In another study, planktonic *A. marina* demonstrated much lower maximum gross photosynthesis values of ~81 μmol O_2 mg Chl d^{-1} h^{-1} and 64 μmol O_2 mg Chl d^{-1} h^{-1} under visible and red light, respectively (18), but these studies did not match the illumination wavelengths to the absorption spectrum of *A. marina* as narrowly as in our study. P_{max} values of >200 μmol O_2 mg Chl d^{-1} h^{-1} were reported in reference 21, studying dense planktonic *A. marina* cultures in a microrespirometer. Diffusion limitations in the alginate matrix coupled with a high cell density of photosynthetically active *A. marina* within the alginate beads account for our finding of steep O_2 gradients similar to those of other photosynthetic biofilms (23). Apparently, the photosynthetic activity of *A. marina* under such conditions was not inhibited.

The use of pulse amplitude-modulated (PAM) fluorometry

TABLE 2 Comparison of relative photosynthetic efficiencies (α) of alginate-embedded and planktonic cells of *Acaryochloris marina*

Growth mode	α (m^2 mg Chl d^{-1})[a]			n[b]	Reference or source
	Blue light	Red light/NIR	Visible light		
Embedded	$(231 \pm 0.22) \times 10^{-6}$	$(268 \pm 0.29) \times 10^{-6}$		3	This study
Planktonic		438×10^{-6}	298×10^{-6}	4	18
Planktonic			205×10^{-6}		42

[a] All measurements are based on three technical replicates, and deviation from the mean is shown for measurements performed in this study.
[b] *n*, number of replicates.

has been established as a valid tool to assess photosynthetic efficiencies in *A. marina* (18). Photosynthesis in immobilized cells of *A. marina* saturated earlier when previously exposed to blue light, while preceding NIR exposure caused a drastic increase in rETR values. No scalar irradiance measurements were performed within beads, and so we can only speculate on the light attenuation capacity of alginate. It is possible that NIR is less attenuated by alginate than blue light, thus penetrating more effectively and deeper into the alginate matrix. Deeper penetration of NIR than of PAR has been reported in coral skeletons (26) and didemnid ascidians (22, 24), which could explain our finding of earlier light saturation under blue light in embedded *A. marina* cells.

More accurate measurements of the efficiency of photosynthetic O_2 production in biofilms of *A. marina* have yet to be performed; such measurements are not trivial as they need, for example, to address the presence of light gradients and combined effects of light scattering and absorption. However, our results provide the first evidence for efficient NIR-driven photosynthesis in *A. marina* when growing in biofilms. It was recently shown that the energy storage efficiency of the photosynthetic light reactions in *A. marina* is comparable to or higher than that of typical Chl *a*-utilizing oxygenic phototrophs (29), suggesting that oxygenic photosynthesis is not fundamentally limited by the photon energies used by *A. marina*. Experimental approaches developed for use in microbial mats (3) showed a relatively low energy storage efficiency of different surface-associated microbial communities at the system level under high-light conditions (4). The same study also revealed higher photosynthetic efficiencies under low-light conditions. Similar studies of energy storage efficiency in *A. marina* biofilms have yet to be carried out.

We showed that alginate-embedded cells of *A. marina* grow well in a dynamic O_2 microenvironment experiencing hyperoxic conditions in the light and hypoxia in darkness. Preliminary microsensor studies of *A. marina* biofilms on the underside of *Lissoclinum patella* showed similar light-dark dynamics in O_2 concentration. Growth in alginate beads may thus be a suitable method for studying *A. marina* under conditions that mimic its natural growth mode and microenvironment in the laboratory under defined and reproducible conditions. This new way of growing *A. marina* also enables metabolic measurements in combination with gene expression studies under various experimental conditions. Such studies could give further insights into potential differential gene expression of *A. marina* in its planktonic and biofilm growth mode, which would provide further information on the niche adaptation and metabolic capabilities of *A. marina* in its natural habitat. It would, for example, be interesting to investigate and compare the microenvironmental regulation of the recently reported N_2 fixation in an *A. marina* isolate (36) under both planktonic and biofilm growth conditions.

ACKNOWLEDGMENTS

This study was supported by the Danish Natural Science Research Council (M.K.) and the Carlsberg Foundation (Denmark).

We thank the staff at Heron Island Research Station for excellent technical support. The Core Facility for Integrated Microscopy (www.cfim.ku.dk) is acknowledged for SEM imaging and image analysis. We thank Erik Trampe for his helpful support in image analysis.

REFERENCES

1. **Akiyama M, et al.** 2001. Detection of chlorophyll *d* and pheophytin *a* in a chlorophyll *d*-dominating oxygenic photosynthetic prokaryote *Acaryochloris marina*. Anal. Sci. **17**:205–208.
2. **Allakhverdiev SI, et al.** 2011. Redox potentials of primary electron acceptor quinone molecule $(QA)^-$ and conserved energetics of photosystem II in cyanobacteria with chlorophyll *a* and chlorophyll *d*. Proc. Natl. Acad. Sci. U. S. A. **108**:8054–8058.
3. **Al-Najjar MAA, de Beer D, Jorgensen BB, Kühl M, Polerecky L.** 2010. Conversion and conservation of light energy in a photosynthetic microbial mat ecosystem. ISME J. **4**:440–449.
4. **Al-Najjar MAA, de Beer D, Kühl M, Polerecky L.** 2012. Light utilization efficiency in photosynthetic microbial mats. Environ. Microbiol. **14**:982–992.
5. **Baker NR.** 2008. Chlorophyll fluorescence: a probe of photosynthesis in vivo. Annu. Rev. Plant Biol. **59**:89–113.
6. **Behrendt L, et al.** 2011. Endolithic chlorophyll *d*-containing phototrophs. ISME J. **5**:1072–1076.
7. **Behrendt L, et al.** 1 December 2011. Microbial diversity of biofilm communities in microniches associated with the didemnid ascidian *Lissoclinum patella*. ISME J. [Epub ahead of print].
8. **Boichenko V, Klimov V, Miyashita H, Miyachi S.** 2000. Functional characteristics of chlorophyll *d*-predominating photosynthetic apparatus in intact cells of *Acaryochloris marina*. Photosynth. Res. **65**:269–277.
9. **Chan Y-W, et al.** 2007. Pigment composition and adaptation in free-living and symbiotic strains of *Acaryochloris marina*. FEMS Microbiol. Ecol. **61**:65–73.
10. **Chen M, Quinnell RG, Larkum AWD.** 2002. The major light-harvesting pigment protein of *Acaryochloris marina*. FEBS Lett. **514**:149–152.
11. **Chen M, et al.** 2005. The nature of the photosystem II reaction centre in the chlorophyll *d*-containing prokaryote, *Acaryochloris marina*. Photochem. Photobiol. Sci. **4**:1060–1064.
12. **Costerton JW, et al.** 1987. Bacterial biofilms in nature and disease. Annu. Rev. Microbiol. **41**:435–464.
13. **Davey ME, O'Toole GA.** 2000. Microbial biofilms: from ecology to molecular genetics. Microbiol. Mol. Biol. Rev. **64**:847–867.
14. **de los Ríos A, Grube M, Sancho LG, Ascaso C.** 2007. Ultrastructural and genetic characteristics of endolithic cyanobacterial biofilms colonizing Antarctic granite rocks. FEMS Microbiol. Ecol. **59**:386–395.
15. **Doron S, Friedman M, Falach M, Sadovnic E, Zvia H.** 2001. Antibacterial effect of parabens against planktonic and biofilm *Streptococcus sobrinus*. Int. J. Antimicrob. Agents **18**:575–578.
16. **Drenkard E, Ausubel FM.** 2002. *Pseudomonas* biofilm formation and antibiotic resistance are linked to phenotypic variation. Nature **416**:740–743.
17. **Duxbury Z, Schliep M, Ritchie R, Larkum A, Chen M.** 2009. Chromatic photoacclimation extends utilisable photosynthetically active radiation in the chlorophyll *d*-containing cyanobacterium *Acaryochloris marina*. Photosynth. Res. **101**:69–75.
18. **Gloag RS, Ritchie RJ, Chen M, Larkum AWD, Quinnell RG.** 2007.

Chromatic photoacclimation, photosynthetic electron transport and oxygen evolution in the chlorophyll *d*-containing oxyphotobacterium *Acaryochloris marina*. Biochim. Biophys. Acta **1767**:127–135.
19. **Jiménez-Pérez MV, Sánchez-Castillo P, Romera O, Fernández-Moreno D, Pérez-Martínez C.** 2004. Growth and nutrient removal in free and immobilized planktonic green algae isolated from pig manure. Enzyme Microb. Technol. **34**:392–398.
20. **Kashiyama Y, et al.** 2008. Evidence for global chlorophyll *d*. Science **321**:658.
21. **Kühl M, Chen M, Larkum AWD.** 2007. Biology of the chlorophyll *d*-containing cyanobacterium *Acaryochloris Marina*, p 101–123. *In* Seckbach (ed), J. Algae and Cyanobacteria in extreme environments, vol 11. Springer, Dordrecht, Netherlands.
22. **Kühl M, Chen M, Ralph PJ, Schreiber U, Larkum AWD.** 2005. A niche for cyanobacteria containing chlorophyll *d*. Nature **433**:820.
23. **Kühl M, Glud RN, Ploug H, Ramsing NB.** 1996. Microenvironmental control of photosynthesis and photosynthesis-coupled respiration in an epilithic cyanobacterial biofilm. J. Phycol. **32**:799–812.
24. **Larkum AWD, Kühl M.** 2005. Chlorophyll *d*: the puzzle resolved. Trends Plant Sci. **10**:355–357.
25. **Lau PS, Tam NFY, Wong YS.** 1998. Effect of carrageenan immobilization on the physiological activities of *Chlorella vulgaris*. Bioresour. Technol. **63**:115–121.
26. **Magnusson SH, Fine M, Kühl M.** 2007. Light microclimate of endolithic phototrophs in the scleractinian corals *Montipora monasteriata* and *Porites cylindrica*. Marine Ecol. Prog. Ser. **332**:119–128.
27. **Marie D, Partensky F, Vaulot D, Brussaard C.** 2001. Enumeration of phytoplankton, bacteria, and viruses in marine samples. Curr. Protoc. Cytomet. **11**:11.11.1–11.11.15.
28. **Marquardt J, Mörschel E, Rhiel E, Westermann M.** 2000. Ultrastructure of *Acaryochloris marina*, an oxyphotobacterium containing mainly chlorophyll *d*. Arch. Microbiol. **174**:181–188.
29. **Mielke SP, Kiang NY, Blankenship RE, Gunner MR, Mauzerall D.** 2011. Efficiency of photosynthesis in a Chl *d*-utilizing cyanobacterium is comparable to or higher than that in Chl *a*-utilizing oxygenic species. Biochim. Biophys. Acta **1807**:1231–1236.
30. **Miyashita H, et al.** 1997. Pigment composition of a novel oxygenic photosynthetic prokaryote containing chlorophyll *d* as the major chlorophyll. Plant Cell Physiol. **38**:274–281.
31. **Miyashita H, Ikemoto H, Kurano N, Miyachi S, Chihara M.** 2003. *Acaryochloris marina* gen. et sp. nov. (cyanobacteria), an oxygenic photosynthetic prokaryote containing Chl *d* as a major pigment. J. Phycol. **39**: 1247–1253.
32. **Mohr R, et al.** 2010. A new chlorophyll *d*-containing cyanobacterium: evidence for niche adaptation in the genus *Acaryochloris*. ISME J. **4**:1456–1469.
33. **Moreira SM, Moreira-Santos M, Guilhermino L, Ribeiro R.** 2006. Immobilization of the marine microalga *Phaeodactylum tricornutum* in alginate for in situ experiments: bead stability and suitability. Enzyme Microb. Technol. **38**:135–141.
34. **Ohashi S, et al.** 2008. Unique photosystems in *Acaryochloris marina*. Photosynth. Res. **98**:141–149.
35. **Pane L, Feletti M, Bertino C, Carli A.** 1998. Viability of the marine microalga *Tetraselmis suecica* grown free and immobilized in alginate beads. Aquac. Int. **6**:411–420.
36. **Pfreundt U, Stal LJ, Vos B, Hess WR.** 12 January 2012. Dinitrogen fixation in a unicellular chlorophyll *d*-containing cyanobacterium. ISME J. [Epub ahead of print].
37. **Ralph PJ, Schreiber U, Gademann R, Kühl M, Larkum AWD.** 2005. Coral photobiology studied with a new imaging pulse amplitude modulated fluorometer. J. Phycol. **41**:335–342.
38. **Resch A, et al.** 2006. Comparative proteome analysis of *Staphylococcus aureus* biofilm and planktonic cells and correlation with transcriptome profiling. Proteomics **6**:1867–1877.
39. **Revsbech NP.** 1989. An oxygen microsensor with a guard cathode. Limnol. Oceanogr. **34**:474–478.
40. **Revsbech NP, BBJørgensen Blackburn TH, Cohen Y.** 1983. Microelectrode studies of the photosynthesis and O_2, H_2S, and pH profiles of a microbial mat. Limnol. Oceanogr. **28**:1062–1074.
41. **Ritchie R.** 2006. Consistent sets of spectrophotometric chlorophyll equations for acetone, methanol and ethanol solvents. Photosynth. Res. **89**:27–41.
42. **Ritchie R.** 2008. Fitting light saturation curves measured using modulated fluorometry. Photosynth. Res. **96**:201–215.
43. **Ruiz-Marin A, Mendoza-Espinosa LG, Stephenson T.** 2010. Growth and nutrient removal in free and immobilized green algae in batch and semi-continuous cultures treating real wastewater. Bioresour. Technol. **101**:58–64.
44. **Sampathkumar B, et al.** 2006. Transcriptional and translational expression patterns associated with immobilized growth of *Campylobacter jejuni*. Microbiology **152**:567–577.
45. **Schliep M, Crossett B, Willows RD, Chen M.** 2010. ^{18}O labeling of chlorophyll *d* in *Acaryochloris marina* reveals that chlorophyll *a* and molecular oxygen are precursors. J. Biol. Chem. **285**:28450–28456.
46. **Schreiber U.** 2004. Pulse-amplitude-modulation (PAM) fluorometry and saturation pulse method: an overview, p 279–319. *In* Papageorgiou GCG (ed), Chlorophyll fluorescence: a signature of photosynthesis. Kluwer, Dordrecht, Netherlands.
47. **Swingley WD, et al.** 2008. Niche adaptation and genome expansion in the chlorophyll *d*-producing cyanobacterium *Acaryochloris marina*. Proc. Natl. Acad. Sci. U. S. A. **105**:2005–2010.
48. **Swingley WD, Hohmann-Marriott MF, Le Olson T, Blankenship RE.** 2005. Effect of iron on growth and ultrastructure of *Acaryochloris marina*. Appl. Environ. Microbiol. **71**:8606–8610.
49. **Theiss C, et al.** 2011. Excitation energy transfer in intact cells and in the phycobiliprotein antennae of the chlorophyll *d* containing cyanobacterium *Acaryochloris marina*. J. Plant Physiol. **168**:1473–1487.
50. **Tomo T, Allakhverdiev SI, Mimuro M.** 2011. Constitution and energetics of photosystem I and photosystem II in the chlorophyll *d*-dominated cyanobacterium *Acaryochloris marina*. J. Photochem. Photobiol. B **104**: 333–340.
51. **Ulstrup K, Ralph P, Larkum A, Kühl M.** 2006. Intra-colonial variability in light acclimation of zooxanthellae in coral tissues of *Pocillopora damicornis*. Marine Biol. **149**:1325–1335.
52. **Van Loosdrecht MCM, Heijnen JJ.** 1996. Biofilm processes, p 255–271. *In* Willaert RG, Baron GV, De Backer L (ed), Immobilised living cell systems: modelling and experimental methods. J. Wiley & Sons, Hoboken, NJ.
53. **Vilain S, et al.** 2004. Comparative proteomic analysis of planktonic and immobilized *Pseudomonas aeruginosa* cells: a multivariate statistical approach. Anal. Biochem. **329**:120–130.
54. **Wang X, Gong Z, Li P, Zhang L.** 2007. Degradation of pyrene in soils by free and immobilized yeasts, *Candida tropicalis*. Bull. Environ. Contam. Toxicol. **78**:522–526.
55. **Wijfels RH, De Gooijer CD, Tramper J.** 1996. Gel immobilised living cell systems: part 2, p 215–236. *In* Willaert RG, Baron GV, De Backer L (ed), Immobilised living cell systems: modelling and experimental methods. J. Wiley & Sons, Hoboken, NJ.
56. **Willaert R.** 1996. Gel immobilized living cell systems: part 1, p 197–213. *In* Willaert RG, Baron GV, De Backer L (ed), Immobilised living cell systems: modelling and experimental methods. J. Wiley & Sons, Hoboken, NJ.